



TECHNISCHE  
UNIVERSITÄT  
WIEN

Project Report

# Preliminary research on an electron beam setup for the QUAK experiment

performed at Atominstitut



at Technische Universität Wien  
Faculty of Physics

under the supervision of  
**Assistant Prof. Dr.rer.nat. Philipp Haslinger**  
and  
**Projektass.(FWF) Dipl.-Ing. Thomas Weigner**

by

**Frank Takara Ebel & Alexander Preimesberger**

Matrikelnummer: 01429282 & 01427641

Stadionallee 2  
1020 Wien

Vienna, 23-01-2021

# Contents

<b>1 Short introduction to QUAK</b>	<b>1</b>
<b>2 Cathodic Ray Tube Basics</b>	<b>2</b>
2.1 Underlying Physics . . . . .	2
2.2 Implementation in the Heerlen D14-363GY . . . . .	5
2.2.1 The Cathode . . . . .	7
2.2.2 Cathode Layout . . . . .	8
<b>3 Cicero Word Generator</b>	<b>10</b>
3.1 Installation of National Instruments drivers . . . . .	10
3.2 Installation of National Instruments Cards . . . . .	10
3.3 Configuring Atticus . . . . .	10
3.3.1 Configure hardware timing / synchronization . . . . .	11
3.4 Configuration and Basic Usage of Cicero . . . . .	12
<b>4 Electron beam setup</b>	<b>13</b>
4.1 Charatarization of a working CRT . . . . .	13
4.2 High Voltage Power Supply HVPS . . . . .	14
4.2.1 Ripple measurement . . . . .	14
4.3 CRT wiring . . . . .	17
4.4 Heater . . . . .	18
<b>5 CRT handling</b>	<b>20</b>
5.1 Opening CRTs . . . . .	20
5.1.1 Rotary tool . . . . .	20
5.1.2 Wire cutting . . . . .	20
5.2 Oxygen poisoning . . . . .	23
<b>6 Vacuum test chamber</b>	<b>26</b>
6.1 Chamber Setup . . . . .	26
6.1.1 CRT mounting mechanism . . . . .	27
6.2 Leak-testing the vacuum test chamber . . . . .	28
6.3 CF-Flange Fastening Algorithm . . . . .	29
<b>7 Deflection Electronics</b>	<b>30</b>
7.1 Demands on the setup . . . . .	30
7.2 Implementation . . . . .	31

<b>8 Beam Characterization</b>	<b>35</b>
8.1 Aluminum foil . . . . .	35
8.2 Faraday cup . . . . .	36
8.3 Deflection frequency . . . . .	37
<b>9 Next Steps</b>	<b>39</b>
<b>References</b>	<b>40</b>

# 1 Short introduction to QUAK

The goal of QUAK (quantum klystron) is to drive Rabi oscillations between hyperfine levels of the potassium atom using a classical electron beam. Suitable isotopes for this experiment are  $^{39}\text{K}$  which has a transition frequency of 461.7 MHz or  $^{41}\text{K}$  with an even lower transition frequency of 254 MHz [1]. For this, it is necessary to DOPPLER-cool the atoms in a MOT. Once the atoms are trapped, they will be exposed to the near-field of the electron beam, which will be spatially modulated with the transition frequency. In order to achieve this goal, the beam must allow for a current of 100  $\mu\text{A}$  and a beam waist of 100  $\mu\text{m}$ .

In our work, we conducted first experiments on how to accomplish an electron beam fulfilling those requirements.

# 2 Cathodic Ray Tube Basics

This chapter features a quick explanation what a Cathodic Ray Tube (CRT) is and what its main components are. This is followed by a more detailed description on how the individual components are implemented in our used CRT, a Heerlen D14-363GY. The chapter ends with a description of the important characteristics of the CRT and the requirement the theory poses on them.

## 2.1 Underlying Physics

“The cathode-ray tube (CRT) is a vacuum tube containing one or more electron guns, the beams of which are manipulated to display images on a phosphorescent screen.”[\[2\]](#)

There are three vital components to accomplish this feat: the electron gun, the electron lens and the deflection plates.

The electron gun generates free electrons from a cathode material, accelerates them onto an anode and thereby produces an electron beam (see fig. [2.1](#)). One important characteristic in the selection of a cathode material is a low work function. It denotes the amount of energy needed to extract one electron from the material. There are two ways to overcome this energy barrier in an electron gun; one can either apply a strong electric field (“field emission”, “cold cathode”) as seen in fig. [2.2b](#). Or one can heat the material until some electrons have enough thermal energy to overcome the energy barrier (“thermal emission”, “hot cathode”, fig. [2.2a](#)). In the case of the cold cathode, a cathode with a sharp tip is used, because the electric field on the surface of a charged conductor is always strongest near sharp points. This causes the electrons to be emitted from the tip and makes for a very point-like electron source.

As our CRT uses a hot cathode, more details on this will be added later along with the description of our cathode’s design.

Normally the cathode itself is covered in beam direction in a so-called Wehnelt cylinder. This part is a conducting cylinder set to a slightly more negative potential than the cathode. It implements two features; firstly, it condenses the emitted electrons, leading to a smaller spot size, i.e. making the cathode a more point-like electron source.

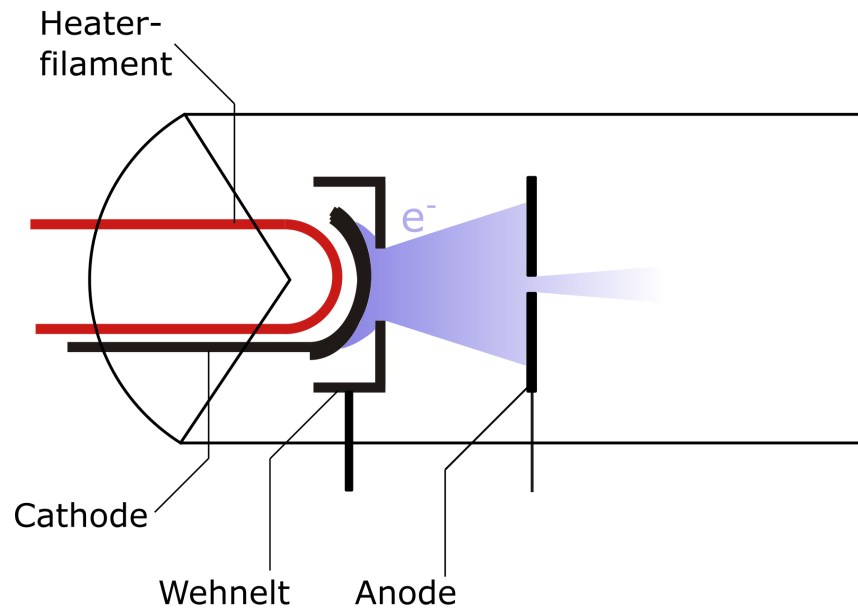
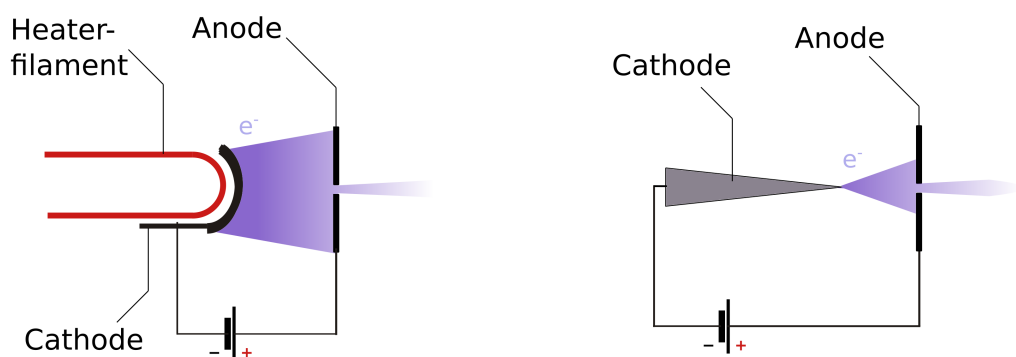


**Figure 2.1:** Schematic of an electron gun.



**(a)** Schematic of a hot cathode.

**(b)** Schematic of field emission cathode.

**Figure 2.2:** Cathode types

Secondly, it enables us to regulate the beam current, the more negative the Wehnelt potential is, the less electrons are emitted by the electron gun. As we make the Wehnelt potential more positive, the beam current increases and continues to rise even after it is more positive than the cathode itself. However, the spot size gets increased, while the proper beam focus is lost.

The electrons that leave the electron gun are still divergent and need to be focused. For our electrons with an energy of 2 keV, an electrostatic lens is used. In their simplest form these are cylindrically symmetrical pieces of conductor, like a ring or tube, set to an electrical potential. By combining several of them, one can create the same effect as a combination of concave and convex lenses [3].

The field of this system is simply governed by Laplace's equation in cylindrical coordinates:

$$0 = \frac{1}{r} \frac{\partial \phi}{\partial r} + \frac{\partial^2 \phi}{\partial r^2} + \frac{\partial^2 \phi}{\partial z^2} \quad (2.1)$$

If we take the axis of the beam to be the  $z$ -axis, the focal point position in the  $x$ - $y$ -plane can be shifted using the two pairs of deflection plates, one for the  $x$ - and one for the  $y$ -direction. The deflection is achieved by applying a voltage between the two parallel plates (see: fig. 2.3). By starting with an electron with kinetic energy  $e \cdot U_0$  which is accelerated in  $x$ -direction by a constant force  $e \cdot U_x/d$  over the extent of the plates  $L$ , the deflection angle is approximately [3]:

$$\delta \approx \tan(\delta) \approx \frac{U_x \cdot L}{2U_0 \cdot d} \quad (2.2)$$

For the measures of our CRT ( $L \approx 5$  cm,  $d \approx 5$  mm,  $U_0 \approx 2$  kV and distance to screen  $\approx 20$  cm) this amounts to a deflection coefficient of around  $20$  V cm $^{-1}$ , which is quite consistent with the value given in the CRT's manual.

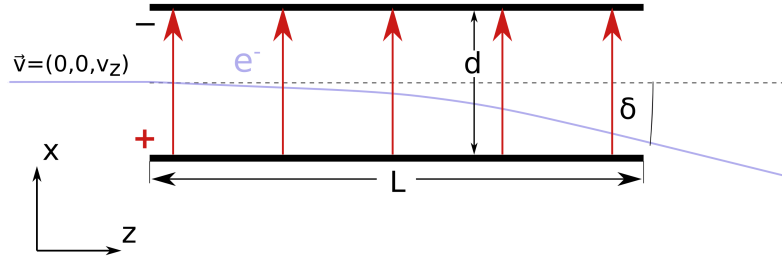


**Figure 2.3:** Deflection of an electron beam in a constant electrical field.

## 2.2 Implementation in the Heerlen D14-363GY

This section describes the CRT that is used in this project: PDS/CRT Heerlen D14-363GY. Figure 2.4a shows an image of said CRT and fig. 2.4b shows a schematic depiction. The cathode is not visible, as it is fixed inside the Wehnelt cylinder (1), just a few millimeters from the exit of the Wehnelt cylinder the electrons pass through the hole in the anode (2), they gain their full kinetic energy over this short distance. The electrons that go through the hole and enter the electrostatic lens, have 2 keV and therefore move at a speed of approximately  $0.08 c$ . The electrostatic lenses are realized using three conducting rings (3), that are set to the same potential but have varying radii: Each consecutive ring has a smaller radius than the previous one.

Between the electrostatic lens and the deflection plates, there is another aperture (4), which is internally connected to the anode and is thereby kept at the same potential. In our setup, the deflection plates are not simply parallel but are shaped like funnels (5,7), between the two pairs of deflection plates, we have the final aperture (6). Its potential can be regulated separately (usually it's on the same potential as the anode)

Finally the beam hits the phosphorous-coated screen which fluoresces on electron impact.

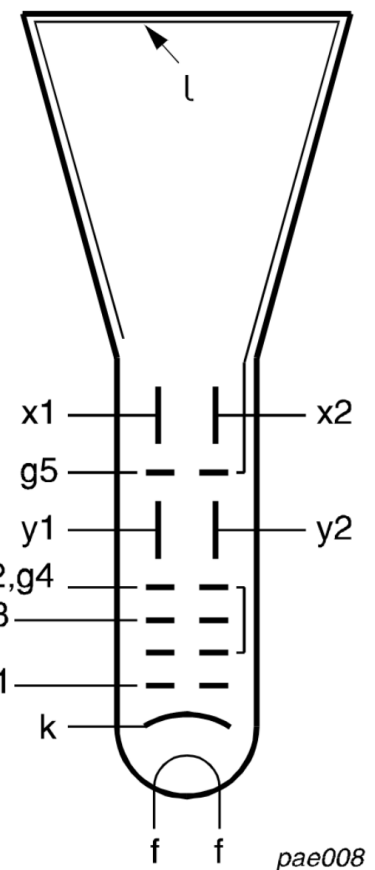
It is connected to the aquadag<sup>1</sup> coating inside the glass envelope and prevents charge building up that could lead to image distortions. Finally, the beam hits the

---

<sup>1</sup>A conductive coating used in CRTs, it consists of graphite particles dispersed in water.



(a) Image picture of the Heerlen D14-363GY



(b) Schematic of the CRT from [4]

**Figure 2.4**

phosphorous-coated screen, which fluoresces on electron impact.

### 2.2.1 The Cathode

As already mentioned, we are using a hot cathode, where electrons are thermally excited to leave the material. Compared to cold cathodes which work by field emission, this leads to a broader energy distribution. For electron microscopy, where a high resolution is the goal, this is undesirable, as it leads to some degree of chromatic aberration in the electron optics; for our purposes this should not be a problem. On the other hand, hot cathodes normally allow for higher current densities. This is very important to QUAK because a high current density allows for a high amplitude of the beam's dipole radiation and therefore a strong coupling to the potassium atoms. The electron current by thermal emission is described by [5, chp 3.2.3]:

$$I = A \cdot T^2 \cdot e^{-b/T} \quad (2.3)$$

Where  $b$  is proportional to the work function of the material,  $T$  is temperature and  $A$  is a material-dependent constant. It is clear from this formula, that a low work function and a high melting point are important characteristics for a good cathode material.

The cathode from one of our Heerlen D14-363GY-tubes has been removed and examined with EDX (Energy-dispersive X-ray Spectroscopy). Nickel, barium, and strontium have been found, which suggests that it is a metal oxide cathode with barium-, strontium-, and possibly aluminum-oxide. This type of cathode is very common in low power electron tubes.

The “Power Vacuum Tubes Handbook” [5, chp 3.5.2.1] describes a typical oxide cathode as a coating of barium and strontium oxides on a structure made from nickel alloys. Nickel is chosen for its strength and toughness, which it retains even at high temperatures. These cathodes are normally made by coating a case structure with a mixture of barium and strontium carbonates (typically 60 % Ba and 40 % Sr), suspended in a binder material and then baking the structure, causing the carbonates to be reduced to oxides.

These metal oxide cathodes normally operate at 700 °C to 820 °C and are capable of average emission densities of 100 mA cm<sup>-2</sup> to 500 mA cm<sup>-2</sup>. Higher peak emissions are possible for shorter periods of time. As already mentioned, one of the advantages of this type of cathode is its high emission current capability compared to cathodes made from other materials. Downsides to this cathode type are its greater susceptibility to so-called oxygen poisoning and to ion bombardment. The literature therefore

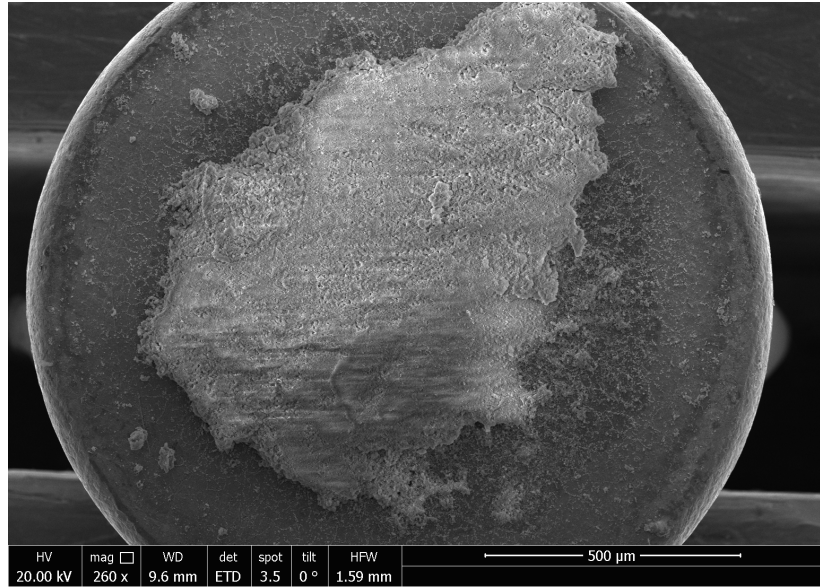


**Figure 2.5:** SEM image of metal oxide cathode.

recommends to avoid prolonged exposure to oxygen. Oxygen poisoning is the process in which oxygen adsorbs onto the cathode and increases its work function, effectively reducing the ability to emit electrons.

Also the material from the oxide cathode will evaporate during the tube's lifetime and will travel to other parts of the tube, adsorbing to electron optics parts and turning them into additional emitters. The literature ([5, chp 3.5.2.1]) therefore, also advises against exceeding the design value for the heater voltage, as this reduces the lifetime of the cathode significantly. CRTs are typically designed to operate for ten years or longer. For QUAK however, a shorter lifetime is acceptable. Therefore during the course of our project, we did drive the cathode with higher heater voltages on various occasions in order to increase the available beam current. We still don't know exactly how fast the degradation due to this effect proceeds; further research is necessary.

### 2.2.2 Cathode Layout

Figure 2.6 shows how metal oxide cathodes for CRTs typically look. The depiction agrees very well with the layout of our cathode. On the image we see the cathode cylinder, which corresponds to the nickel support structure mentioned above. It is shaped into a cup, in which the heater filament (shaped into a coil) is inserted. The oxide disk, from where the electrons are emitted, is baked onto the top of the cathode cylinder. The cathode cylinder is mounted on an isolating support structure and

## 2 Cathodic Ray Tube Basics

---

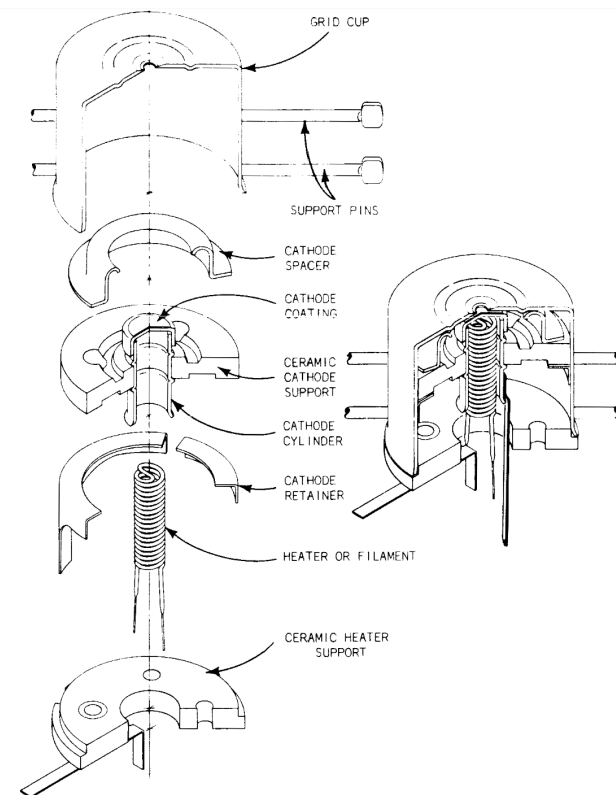


**Figure 2.6:** Schematic of the layout of a typical CRT-cathode [6].

inserted into the Wehnelt cylinder, which is called “grid cup” in the drawing.

# 3 Cicero Word Generator

This chapter describes the installation and initial setup of Cicero Word Generator [7] on a PC running Windows 10 with analog and digital cards from National Instruments (NI). The code is freely available on GitHub [8]. This chapter contains only differences, problems, and possible solutions encountered when Cicero was installed for the PC ‘Fritz Fantom’ which will be used for the QUAK experiment. It is therefore advised to use the technical and user manual [9] in conjunction.

## 3.1 Installation of National Instruments drivers

Before setting up the Cicero Word Generator, it is necessary to install the newest .NET Framework [10] from Microsoft. Then NI drivers, NI-DAQmx (version 9.3), NI-VISA (newest version), and NI-4888.2 (newest version) should be downloaded from the National Instruments website [11] and installed. When installing the NI drivers it is possible to get an ‘Runtime Error!’. In this case it is necessary to set the Regional format settings of Windows 10 to ‘English (United States)’ [12].

## 3.2 Installation of National Instruments Cards

After installation of the necessary drivers, the physical cards can be inserted in the PCIe slots on the motherboard. On ‘Fritz Fantom’ a digital card (NI PCIe-6537B) was installed on PCIe bus 3 while two analog cards (both NI PCIe-6738) were installed on PCIe bus 4 and 5.

## 3.3 Configuring Atticus

After installation of the NI cards, Atticus should be launched for the first time and closed without changing any settings. After this, the NI-DAQmx drivers should be updated to the newest version. If version 9.3 was not used when launching Atticus

in this step, it could result in an error. After this, “Configuring Atticus” on the user manual can be followed. The **Server Name** was set to ‘Fritz\_Fantom’. **Dev1** to **Dev3** were set in the same ascending order as the physical installation on the motherboard.

### 3.3.1 Configure hardware timing / synchronization

For synchronization, a **Shared Sample Clock** was used with **Dev1** being the master card. The settings are summarized in table 3.1 and table 3.2. **Dev3** follows the same settings as **Dev2** except ‘SampleClockExternalSource’ was set to ‘/Dev3/RTSI7’. The ‘SampleClockRate’ is set to 350 kHz since this is the fastest rate with all 32 analog channels active. It is possible to raise this to 1 MHz by only using 8 channels (1 channel per bank).

To route the clock signal to the timing bus, under ‘Connections’ the ‘Destination Terminal’ was set to **/Dev1/RTSI7** and ‘Source Terminal’ to **/Dev1/DO/SampleClock**.

**Table 3.1:** Settings for **Dev1**.

Setting	Value
MasterTimebaseSource	
MySampleClockSource	DerivedFromMaster
SampleClockRate	350000
UsingVariablenamebase	False
SoftTriggerLast	True
StartTriggerType	SoftwareTrigger

**Table 3.2:** Settings for **Dev2**.

Setting	Value
MasterTimebaseSource	
MySampleClockSource	External
SampleClockExternalSource	/Dev2/RTSI7
SampleClockRate	350000
UsingVariablenamebase	False
SoftTriggerLast	False
StartTriggerType	SoftwareTrigger

## 3.4 Configuration and Basic Usage of Cicero

After setting up the Atticus server, Cicero can be configured. In step 3.c. it is necessary to write the full IP address and not ‘localhost’.

### Saving of Settings and Sequences

The ‘SettingsData’ of the Server Atticus are saved in C:\Users\confetti\Documents\Atticus\SettingsData while the ‘SequenceData’ of Cicero are saved in C:\Users\confetti\Documents\Cicero\SequenceData.

### Sequence length limit

The duration of a sequence is limited to  $2^{32}/(16 * 32 * 350 \text{ kHz}) = 23.967 \text{ s}$  coming from a 32-bit application, 16 bit per channel, 32 channels in a NI PCIe-6738 card, and 350 kHz clock rate.

# 4 Electron beam setup

## 4.1 Charatarization of a working CRT

HAMEG HM507 oscilloscopes [13] were used for testing purposes. These contain a D14-363GY/123 [4] CRT. Although it only has a bandwidth of 0 MHz to 50 MHz, which is not sufficient to reach the hyperfine splitting frequency of 461.7 MHz for  $^{39}\text{K}$  [1] (or 254 MHz for  $^{41}\text{K}$ ), it was used nevertheless because of its simple construction and availability. The back pin arrangement is shown in fig. 4.1.

The voltages and currents of the pins to drive the CRT were measured using a 2.5 kV probe with a voltage divider of 100:1 and are summarized in table 4.1. It was not possible to measure pin g3 directly. Therefore a HVPS (section 4.2) was used to set a voltage and the beam diameter was observed. The best focus was achieved with the value written in the table. The voltage offset of x-, and y-plates was not possible to measure directly, since it varies with time to draw the necessary image on the phosphor screen. The given values are the mean of the minimum and maximum measured voltage. The deflection coefficient is summarized in table 4.2.

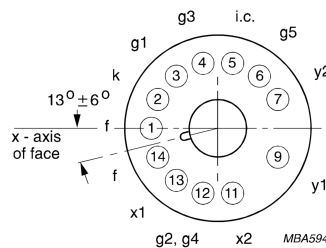


**Figure 4.1:** Pin arrangement, bottom view [4].

**Table 4.1:** D14-363GY/123 CRT pin measurements.

number	pin	voltage/V	current/ $\mu$ A
1	f	$-1.99 \times 10^3$	$86.6 \times 10^3$
2	k	$-2.00 \times 10^3$	-7.6
3	g1	$-2.03 \times 10^3$	0
4	g3	$-1.813 \times 10^3$	0
5	i.c.	71.7	0.1
6	g5	64.0	7.2
7	y2	78	-
9	y1	78	-
11	x2	96	-
12	g2, g4	71.0	0
13	x1	96	-
14	f	$-1.97 \times 10^3$	$-86.2 \times 10^3$

**Table 4.2:** D14-363GY/123 deflection coefficients [4].

horizontal	$M_x$	19 V/cm
vertical	$M_y$	11.5 V/cm

## 4.2 High Voltage Power Supply HVPS

To produce high dc voltages to drive the CRT, four HCP 14-6500 power supplies [14] were used. They were named ‘HVPS 1’ to ‘HVPS 4’ and can provide up to 2 mA at  $\pm 6.5$  kV. To connect the output to the CRT pins, BNC cables were refitted with a save high voltage (SHV) connector on one side while on the other end the BNC connector was kept (fig. 4.2). A 6 kV probe was used to obtain the breakdown voltage, which is around 3 kV caused by the coaxial cable which was not built do sustain high voltages.

### 4.2.1 Ripple measurement

Each power supply was measured for its ripple with a set voltage of 2 kV. A 2.5 kV probe (attenuation ratio 100:1) was connected to an oscilloscope set to ac coupling with a timescale of 1 ms. To get the electronic noise of the oscilloscope itself, the probe was shorted and the noise measured. A picture of a measurement is shown in fig. 4.3 with the values summarized in table 4.3. As can be seen, the ripple is very close to the noise level and can not really be distinguished.

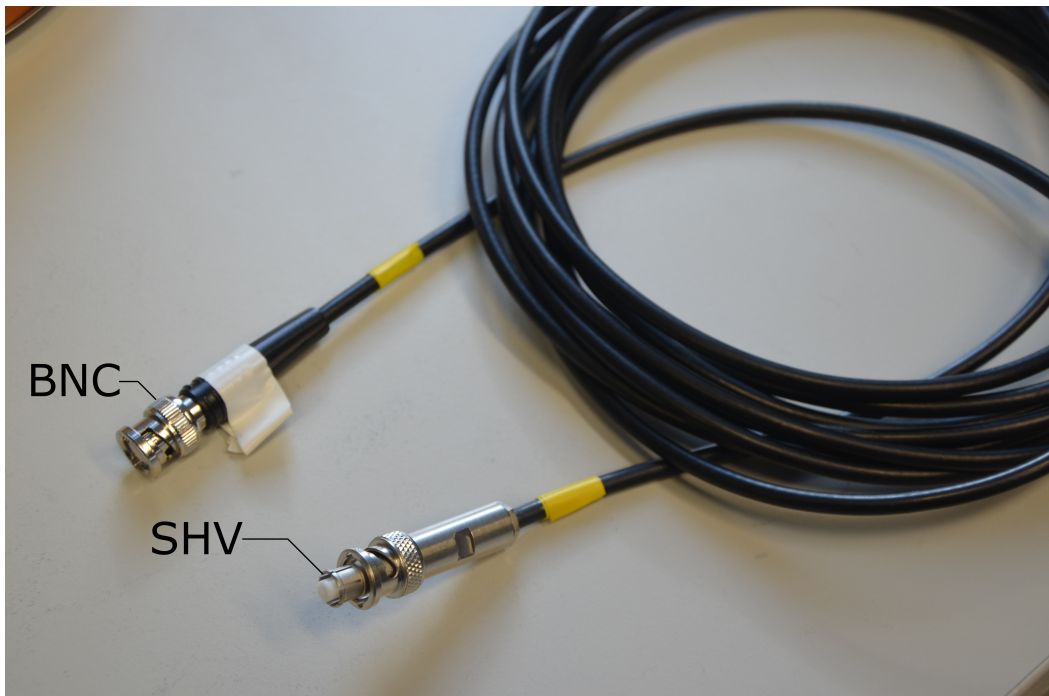


**Figure 4.2:** Coaxial cable with SHV and BNC connector.

**Table 4.3:** HVPS ripple

device	ripple/mV
short	116
HVPS 1	136
HVPS 2	138
HVPS 3	194
HVPS 4	204

#### 4 Electron beam setup

---

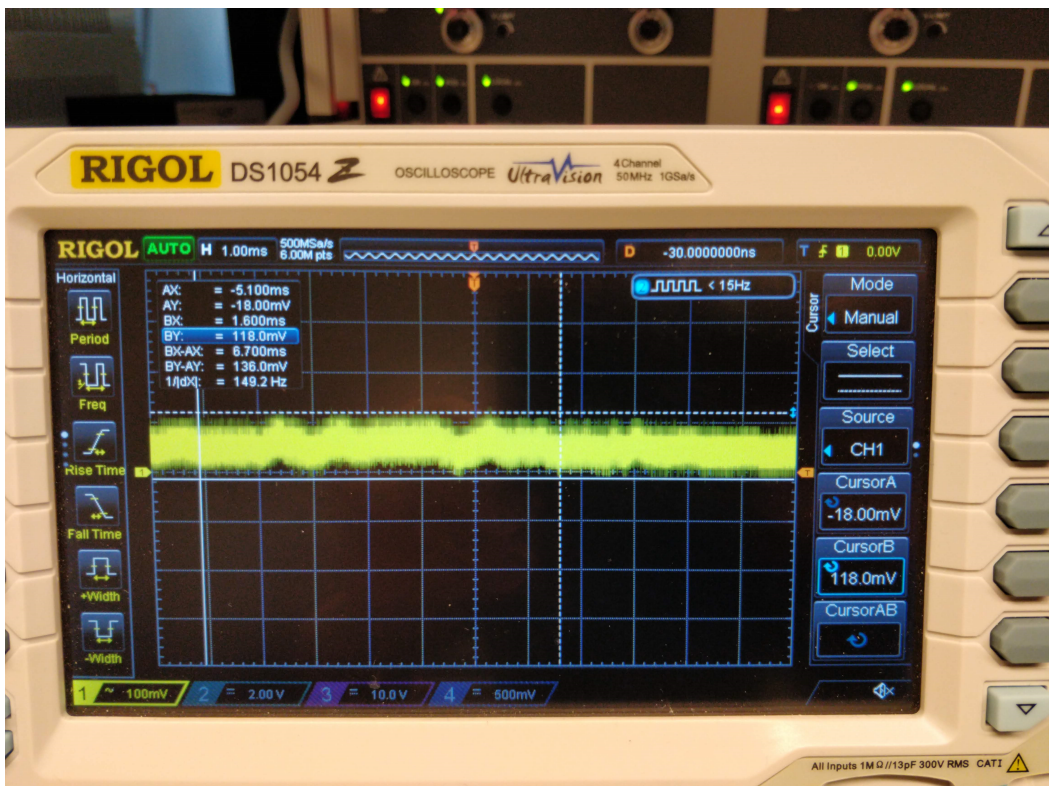


**Figure 4.3:** Measurement of HVPS ripple.

### 4.3 CRT wiring

A schematic of the supplied power is shown in fig. 4.4. The pin i.c. stands for internally connected and is wired to pin g2, g4. A small ac or dc voltage is necessary to drive the heater filament f. This part of the setup is explained in section 4.4.

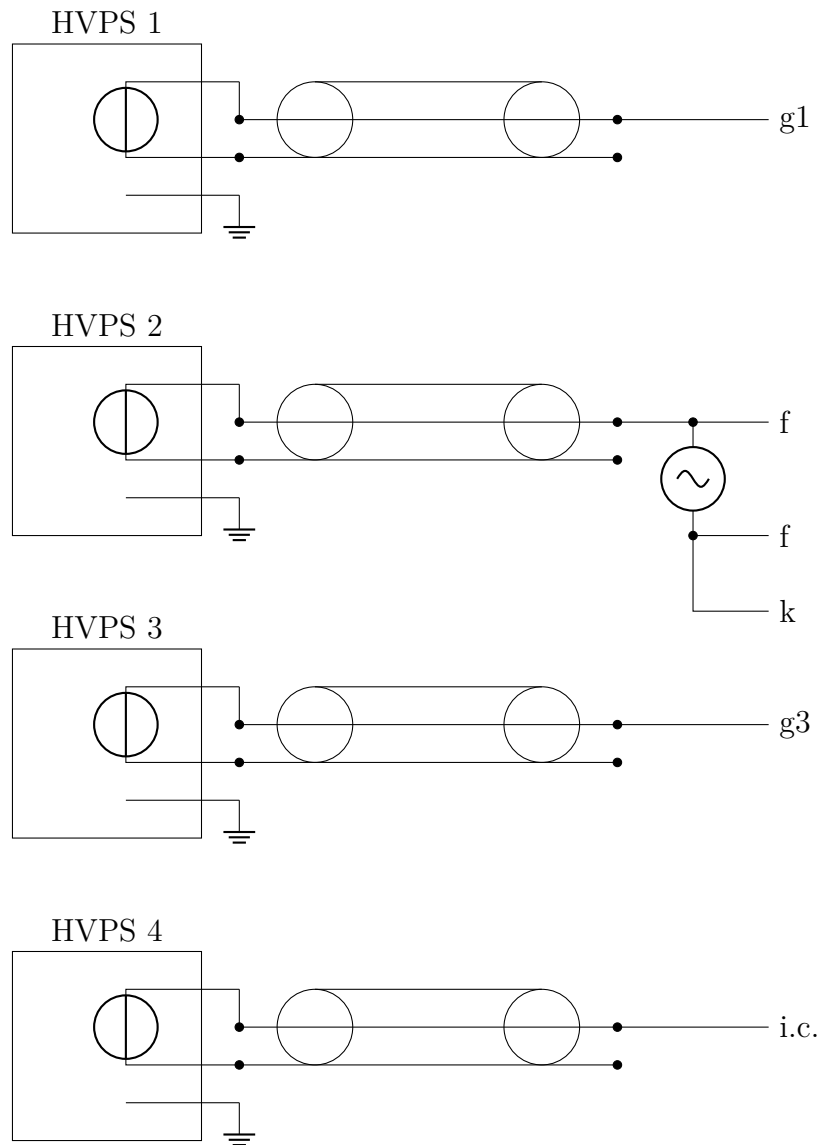
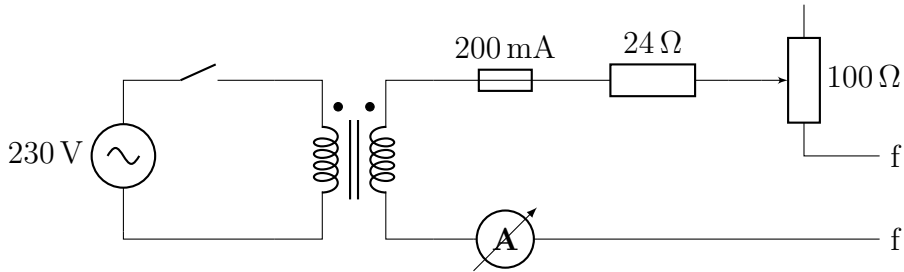
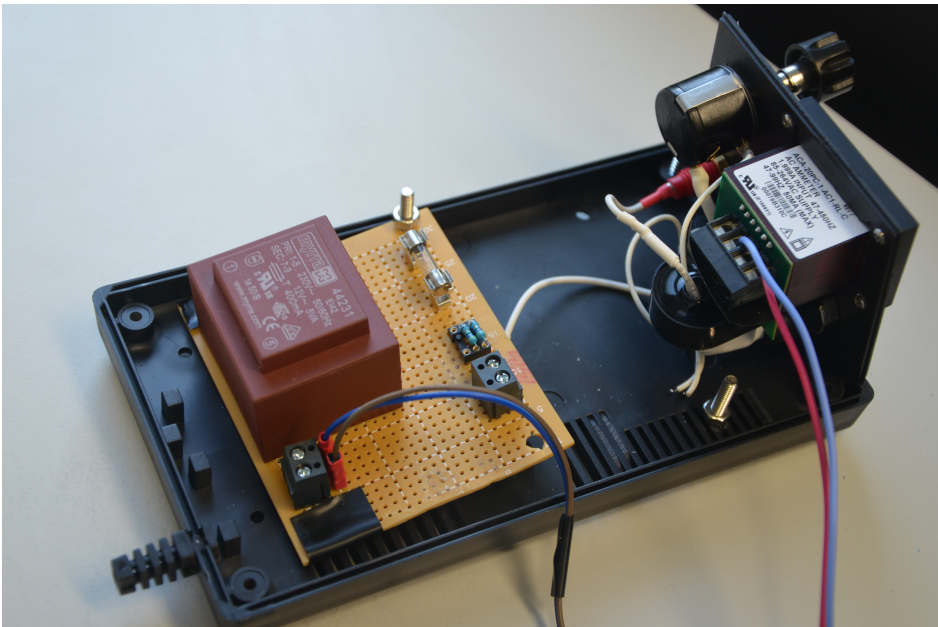


**Figure 4.4:** Schematics of supplying CRT pins with power.



(a) Circuit diagram of filament power supply.



(b) Picture of built filament power supply.

**Figure 4.5:** AC power supply used to heat the filament with a  $-2\text{ kV}$  bias voltage.

## 4.4 Heater

The heater provides an adjustable ac voltage, which is used to regulate the temperature of the cathode. In the cold state, the heater filament has an electrical resistance of approximately  $15\ \Omega$ . When heated, its value rises to  $90\ \Omega$ . The normal heater voltage for the D14-363GY/123 during operation is 6.0 V to 6.6 V according to [4]. Our ac-power supply (shown in figure 4.5) consists of an isolation transformer (from grid voltage to 12 V). Its primary and secondary circuits are isolated up to 4 kV [15]. The power supply has two banana plug sockets to connect to the heater filament. It is connected to the transformer in series with a  $100\ \Omega$  potentiometer. Using the full resistance, there

#### 4 Electron beam setup

---

is a voltage of approximately 5.7 V applied to the heater filament, by lowering the resistance this value goes up to nearly the full voltage of the transformer. The current running through the filament is measured with an integrated ampere meter [16], that measures currents up to 2 A with mA accuracy.

At the beginning of operation it is recommendable to set the maximum resistance and slowly increase the current to the desired value once the filament is heated up. As the resistance of the cold filament is significantly lower, high onset currents could otherwise damage it.

# 5 CRT handling

## 5.1 Opening CRTs

In order to have a free electron beam in the experimental setup to influence cold potassium atoms, it is necessary to cut open the CRT. This section explains the different methods which were tried and which resulted in clean and easy cuts. All slices were made in a glove box filled with nitrogen gas (fig. 5.1) to reduce oxygen poisoning of the cathode.

### 5.1.1 Rotary tool

First, a small hole was drilled in the center of the CRT pins to pressurize the CRT with nitrogen. Then a diamond wheel attached to a rotary tool was used to cut the glass. This method was tried twice, but did not work well. A lot of glass dust was produced, which adhered to the electron optics. Another obstacle is the plastic box, since it is not fully transparent and therefore made more difficult to see inside.

### 5.1.2 Wire cutting

Higher success was achieved by cutting the glass with a heated wire. Two wires were put through the glove box, each ending in a ring terminal. A small height adjustable stage was built out of optic element mounts (fig. 5.2) in which the CRT was put vertically and looped by an 0.25 mm steel wire (Fe 70/Cr 25/Al 5). It is important to keep a small gap in the loop to avoid an electrical short. Therefore two notches were made in which the wire was fixed.

The assembly was put inside the glove box, which was subsequently filled with nitrogen. A current of approximately 2 A to 2.5 A was used to heat the thin wire which resulted in a breaking point inside the CRT glass. This method does not require a CRT pressurization before the cut. In order to not destroy a device by mistake, this procedure was first extensively tested on drinking glasses.

## 5 CRT handling

---



**Figure 5.1:** Glovebox filled with nitrogen gas to open CRTs.

## 5 CRT handling

---



**Figure 5.2:** Stage to cut CRT with wire.

## 5.2 Oxygen poisoning

As mentioned in chapter 2 it is paramount to avoid contact of the cathode with oxygen. Therefore tests with a broken CRT were made to test on how well it can be isolated from air.

The first experiment consisted of filling a drinking glass put upside-down with helium and putting a lighter after a set amount of time. If the fire goes off, it means that oxygen did not get inside. This was tested successfully from 0.5 min to 10 min.

Next, plastic wrap was put on top of the glass filled with nitrogen by a rubber band. The glass was put with the open side up from 3 min to 10 min after which it was turned upside down and the foil was removed. A lighter was put inside and the flame went out again.

To improve the precision, a He leak tester was used. For the first two tests, one plastic foil and one rubber band were used; for the third test three foils and two rubber bands; and for the last test an aluminum foil was hot glued on the CRT to seal it. The measurement locations are shown in fig. 5.3. For the glued seal, leakage was measured on the whole circumference. In table 5.1 ‘glue avg’ denotes the average leak rate of this measurement while ‘glue max’ describes the highest value. A seal with rubber band and clear foil tend to higher leakage. Based on these measurements it is recommended to use glued aluminum. But care needs to be taken in order ensure that the whole CRT is sealed since even a small leak can result in a rate around an order of magnitude above the background.

## 5 CRT handling

---

**Table 5.1:** He leak test.

location	leak rate/(10 <sup>-5</sup> mbar l/s)
1 plastic foil, 1 rubber band	
background	8
plastic foil	20
He gas cylinder	200
1 plastic foil, 1 rubber band	
background	7
plastic foil	20
rubber band	40
3 foils, 2 rubber bands	
background	20
plastic foil	30
rubber band	70
1 aluminum foil, hot glue	
background	6
glue avg	7
glue max	60
aluminum foil	8

## 5 CRT handling

---



(a) plastic foil



(b) rubber band



(c) glue



(d) aluminum

**Figure 5.3:** Measurement locations of He leakage.

# 6 Vacuum test chamber

Since the QUAK experiment will use cooled potassium atoms, a vacuum chamber is necessary. The goal of our preliminary setup was to only test and characterize the electron beam without the presence of trapped atoms. Low pressure is necessary to provide a mean free path long enough so that electrons do not scatter too much. It was important to have the possibility to use the phosphor coated CRT screen inside our chamber. Therefore CF160 flanges were chosen.

## 6.1 Chamber Setup

A 3D render of the chamber is shown in (fig. 6.1). The center piece consists of a 6-way cross with view ports at the front and bottom. A valve was installed at the back in order to flood the chamber with nitrogen (Alphagaz<sup>TM</sup>, N<sub>2</sub> purity  $\geq 99.999\%$ ) when installing a new CRT to avoid water vapor getting into the chamber. On the right side, a HiCube 300 Eco turbo pump was installed. To the left, a wobble stick was attached with a wire to move items inside the running chamber. Later, a Faraday cup was attached to it (see section 8.2 for more information). A straight CF160 pipe of length 27 cm was installed at the top with a 5 port cluster flange, each being of type CF40.

In the middle port, a Thycracont VSH89DL pressure gauge was installed. On the left, a MIL 19 C connector was installed to supply the necessary voltages to the CRT. Two flanges were equipped with four BNC feedthroughs each. One of them was used to connect the x-, and y-plates, while the other connected to the wobble stick and aluminum foil at the CRT screen. Further explanation will be given in chapter 8. The last port was capped off by a blank flange.

For the inside wires, at first stranded copper cables were used. These were later swapped for Kapton insulated BNC cables. The chamber was sealed by Viton rubber gaskets which were changed to copper gaskets. Only the gasket at the cluster flange was kept to rubber since the chamber was opened and closed multiple times at that connection.

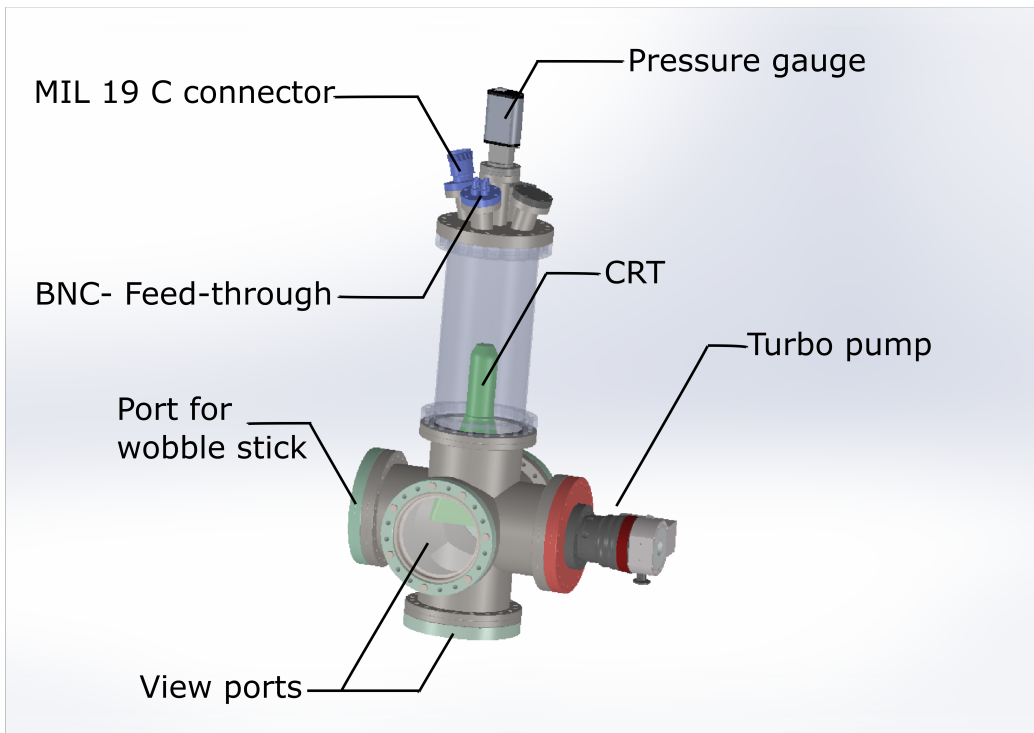


**Figure 6.1:** 3D rendering of test chamber.

### 6.1.1 CRT mounting mechanism

Two M8 rods of length 66 cm were screwed with a counter nut into the cluster flange. On each, a L shaped aluminum piece was installed between two nuts. These were then connected by a hose clamp, which was used to secure the CRT inside below the cluster flange (fig. 6.2).



**Figure 6.2:** Image of CRT mounting mechanism.

## 6.2 Leak-testing the vacuum test chamber

Before inserting a CRT for the first time, measurements were made in order to find out how well low pressure could be maintained inside the setup. First, the chamber was set to a pressure of  $10^{-5}$  mbar after which the pump was turned off. The pressure was measured once a minute for a duration 3 h. This is shown in fig. 6.3.

Without a CRT installed, it was possible to reach a pressure of  $6.8 \times 10^{-7}$  mbar. With a CRT installed inside, the lowest achieved pressure was  $2.0 \times 10^{-6}$  mbar. It was not possible to reach a lower pressure due to outgassing. As mentioned in section 6.1, changes were made to the chamber. Thanks to these, it was possible to reach a pressure of  $1.2 \times 10^{-7}$  mbar with a CRT inside the setup.

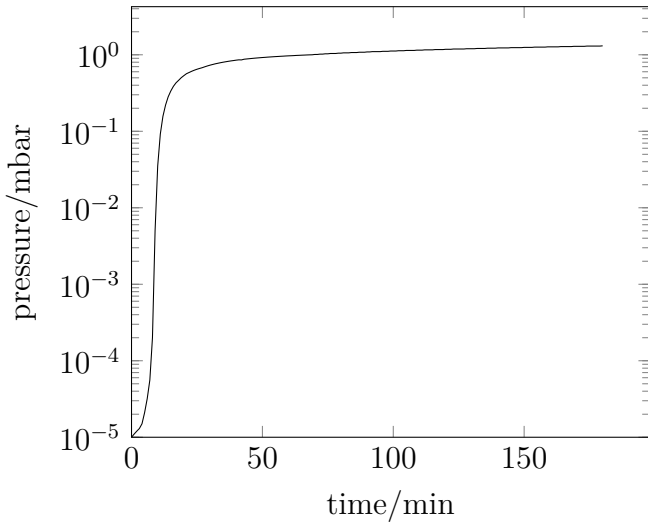


**Figure 6.3:** Time evolution of pressure inside the test chamber after turning off pump.

### 6.3 CF-Flange Fastening Algorithm

When attaching flanges, it is important to start with a low torque and to fasten opposite screws to prevent too much force on one side of the gasket. For M6 screws, the torque was incrementally set to 6 N m, 10 N m, 15 N m and 20 N m and for M8 screws 8 N m, 16 N m and 25 N m. After finishing every opposite screw pair at a set torque, the procedure was repeated twice before going to a higher torque. This was done in order guarantee a tight and even seal.

# 7 Deflection Electronics

## 7.1 Demands on the setup

For the QUAK experiment it is paramount to be able to deflect a beam of a sufficient current precisely at the right frequency with a sufficiently small bandwidth. As previously mentioned, our deflection system simply consists of two pairs of parallel plates between which a voltage is applied. Controlling this voltage allows us to control the deflection of the beam. Various aspects are important here (illustrated in fig. 7.1):

**Offset:** Although the deflection of the beam is controlled by the voltage between the plates, it is necessary to be able to set their mean potential as well. During normal operation this offset voltage is at 96 V for the x-direction and at 78 V for the y-direction. These offsets are necessary to keep the beam focused.

**Amplitude:** The deflection coefficients in the x and y planes are  $19 \text{ V cm}^{-1}$  and  $11.5 \text{ V cm}^{-1}$  respectively (see [4]). We therefore need to be able to supply up to 100 V in order to be able to move the beam in a large enough area.

**Frequency:** The final goal is to be able to deflect the beam at the hyperfine splitting frequency of  ${}^{39}\text{K}$ , which is 461.7 MHz or  ${}^{41}\text{K}$ , with a frequency of 254 MHz. This is likely to prove impossible with this CRT-model, observations at the highest frequency we have tried so far will be discussed in section section 8.3.

**Waveform:** Ultimately we want the cold atoms to experience a field that oscillates like a sine wave. As a first try it is therefore reasonable to apply a sinusoidal voltage.

**Lissajous curves:** Having the ability to control the deflection in both the x- and the y- axis, allows us to have our beam draw out Lissajous Curves (fig. 7.2). By applying sine waves of equal frequency to both pairs of deflection plates and by being able to control the phase between them we can have the beam oscillate on a straight line or a circle. This allows us to generate either a linearly or circularly polarized field.

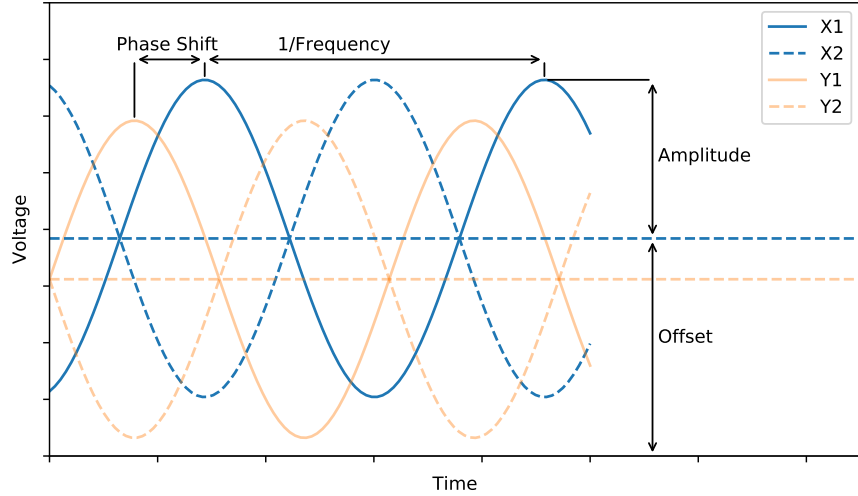


**Figure 7.1:** Characteristics of the generated deflection voltages.

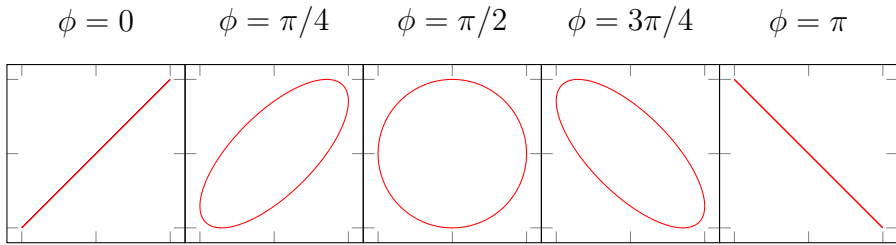


**Figure 7.2:** Lissajous Curves.

## 7.2 Implementation

A first setup with which we can try to obtain the desired voltages is depicted in fig. 7.3. On the very left we have a signal generator that is capable of producing the right frequency (461.7 MHz) this signal is then split up into an x-, and a y-branch. One of the two branches is connected to a phase shifter, which is able to delay the input signal by up to  $200^\circ$ , allowing us to set any desired phase shift between x-, and y-deflection and to correct for inadvertent delays from the other electronics. Both the x-, and y-signal are then amplified using Mini Circuits ZHL amplifiers. In the final step, a center tapped transformer allows us to produce voltages for the plates X1 and X2 (or Y1 and Y2 respectively) with a phase shift of exactly  $180^\circ$  between them. By setting the center tap to the desired offset potential, we should get the voltage curves described above. To understand this setup in more detail, it is useful to examine its

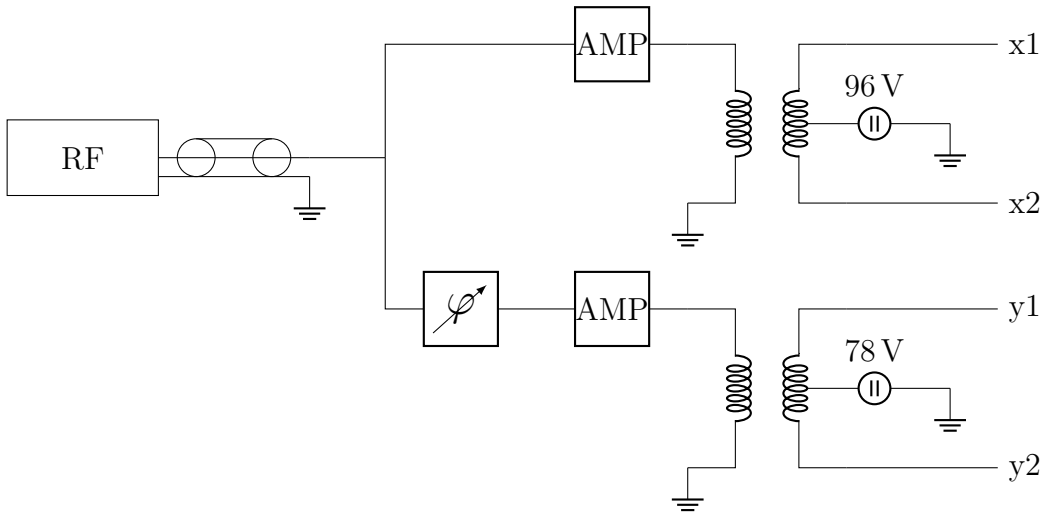


**Figure 7.3:** Deflection circuit.

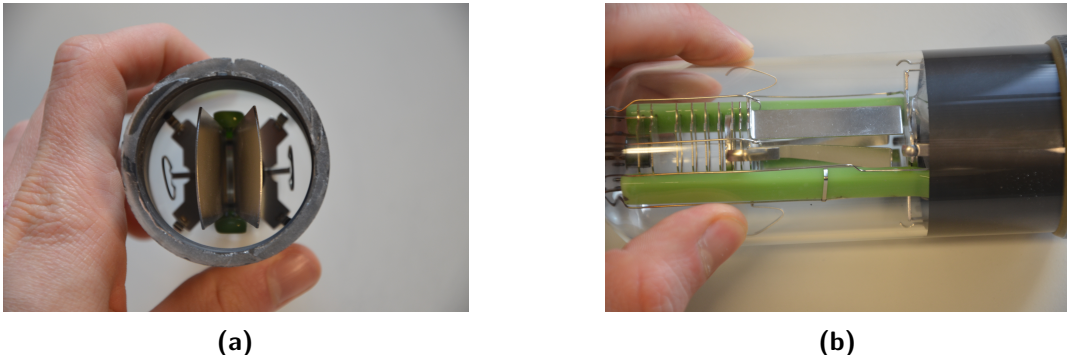


**Figure 7.4:** Images of deflection plates.

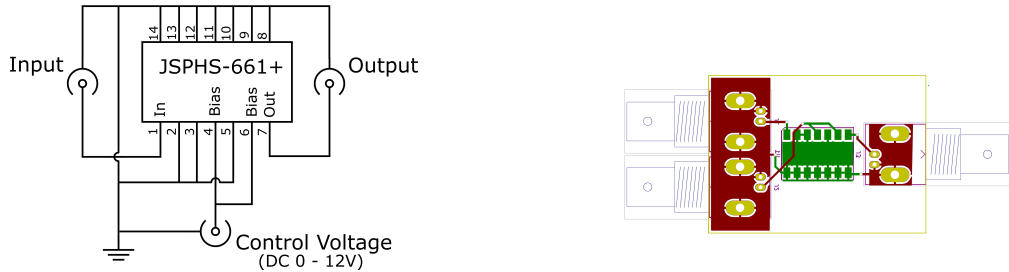
most important parts more closely:

**Amplifier:** Up to now we have used the Mini Circuits ZHL 32A [17] and the ZHL 1A [18] amplifier, which have a fixed gain of 25 dB and 16 dB respectively. Inputs and outputs can simply be connected via BNC cables. The amplifier is powered by a linear power supply with a DC voltage of 24 V via two banana plugs in the front. Since we want to control the Lissajous curves shapes (as the deflection coefficients for the x- and y- plates differ), it is desirable to be able to adjust the amplifier gain in future versions of the setup.

**Center Tapped Transformer:** The center tapped transformer we use is the Mini-Circuits TC8-1G2+ ([19]), a transformer for frequencies between 2 MHz to 500 MHz, with an impedance ratio of 8. Figure 7.7 shows how the center tapped transformer is implemented. The in- and outputs, as well as the bias voltage

can be connected via BNC cables. As usual, the shields of all these cables are connected to ground, furthermore they are connected to each other and to the housing. As a safety feature, both outputs X1 and X2 are directly connected to the bias through an arrangement of diodes: Two connections, each with a normal diode and a Zener diode facing in opposite directions. The breakthrough voltage of the Zener diode is 200 V, during normal operation the voltage on it stays below this value and none of the connections let any current through as one of the two diodes is always blocking it. However if one of the plates in the CRT accidentally comes in contact with high voltage, the connection with the appropriately oriented Zener diode opens up, preventing a voltage spike on the center tapped transformer and thereby protecting the electronics connected to its primary circuit. At the point of writing there are still some problems with the behavior of the center tapped transformer, the capacitance of the diodes introduces an undesired phase shift between the two signals. Figure 7.6a shows the circuit's behavior at 465 MHz without its diodes, here the signals are shifted by  $120 \text{ ps} \hat{=} 20^\circ = 0.35 \text{ rad}$ . Additionally, applying a bias voltage leads to differing amplitudes, as can be seen in fig. 7.6b.

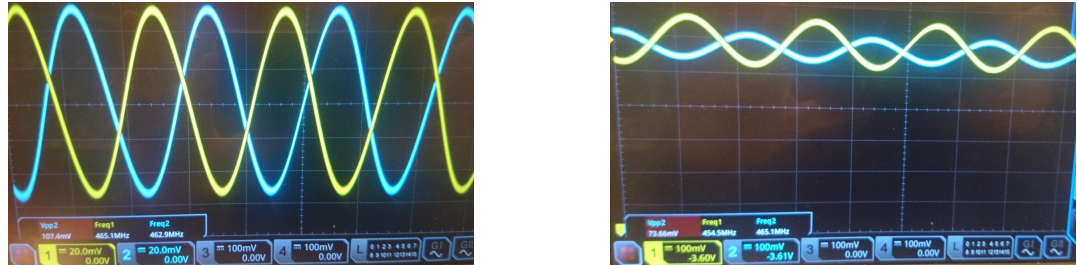
**Phase Shifter:** To control the phase shift between the x- and y-deflection plates, we use a Mini-Circuits [20] phase shifter. This part was put in a housing ([21]) on a separate PCB and can be connected via BNC cables. Figure 7.5a shows how the phase shifter is connected and fig. 7.5b shows the corresponding PCB layout. Note that again the shields of the BNC cables are connected among each other and to the housing. The JSPHS-661+ is designed for frequencies in the range 400 MHz to 600 MHz. By applying a DC voltage of 0 V to 12 V to the bias connector, it is possible to introduce a phase shift of up to  $200^\circ$  to the signal.



(a) Schematic of phase shifter connections.

(b) PCB-Layout of the phase shifter.

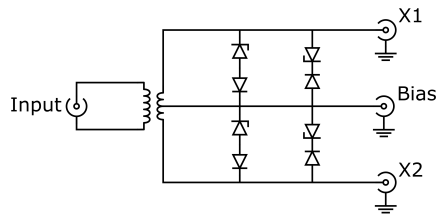
**Figure 7.5**



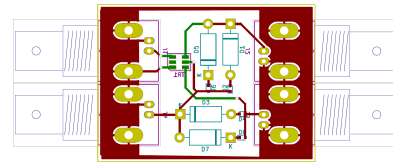
**(a)** Signal of center tapped transformer without diodes, unbiased at 465 MHz.(1 ns/division horizontally and 20 mV/division vertically)

**(b)** Signal of center tapped transformer without diodes, biased at 465 MHz.(1 ns/division horizontally, 100 mV/division vertically, -3.6 V offset)

**Figure 7.6**

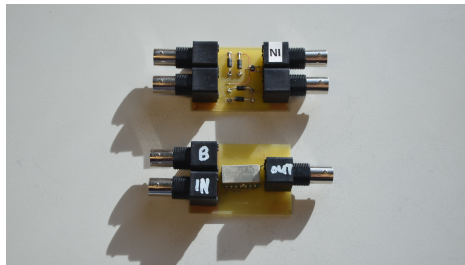


**(a)** Schematic of center tapped transformer connections.



**(b)** PCB-Layout for center tapped transformer.

**Figure 7.7**



**(a)** Finished PCBs.



**(b)** Finished PCB in housing.

**Figure 7.8**

# 8 Beam Characterization

## 8.1 Aluminum foil

In fig. 8.1 the inside of the 6-way cross of is shown. On one side of the phosphor screen, aluminum foil was attached to simulate the aquadag coating inside the cut CRT. The beam was deflected on the aluminum foil and the BNC output was connected to ground through an ammeter to measure the beam current. As shown in fig. 8.2 there is close to no difference in the filament voltage (and therefore heating power) between an opened and sealed CRT while the beam current on the aluminum foil varies widely. One possible reason could be that electrons scatter. Therefore, a Faraday cup (see section 8.2) was used.



**Figure 8.1:** Front view of vacuum chamber.

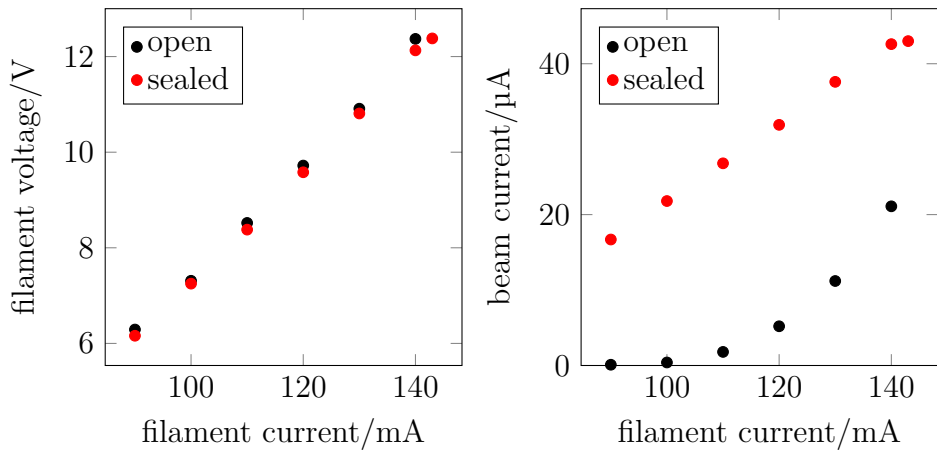


**Figure 8.2:** Difference in filament voltage and beam current between an open and sealed CRT.

## 8.2 Faraday cup

In order to accurately measure the full beam current, a Faraday cup was built. A schematic is shown in fig. 8.3. A copper tube was cut at an  $45^\circ$  angle on one side and a Cu-sheet was soldered at the top and bottom. A small hole of around 5 mm was drilled at the top and a coaxial cable was attached on the mantle which connects to a BNC feed through at the top of the chamber. The small opening and angled floor were added, in order to reduce electron loss through back scattering, as indicated by blue arrows in fig. 8.3. At the top surface a phosphor coating was applied, in order to make the beam visible. This made it easier to guide it into the opening hole.

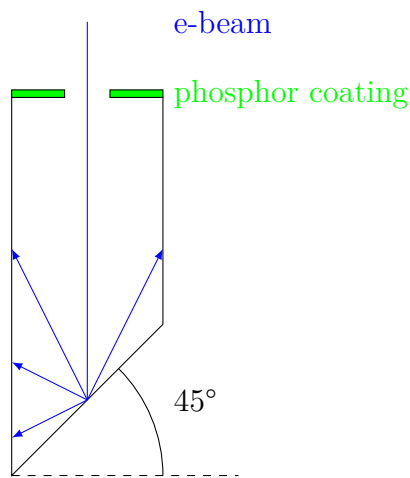


**Figure 8.3:** Schematics of Faraday cup.

With this improved setup, the beam current was measured again (fig. 8.4). It can be seen, that a current of over  $300 \mu\text{A}$  was achieved, which is more than the necessary amount for the experiment. However, through this measurement it became evident that the current is not stable. A measurement on the next day under the same settings resulted in a current between  $50 \mu\text{A}$  to  $120 \mu\text{A}$ .

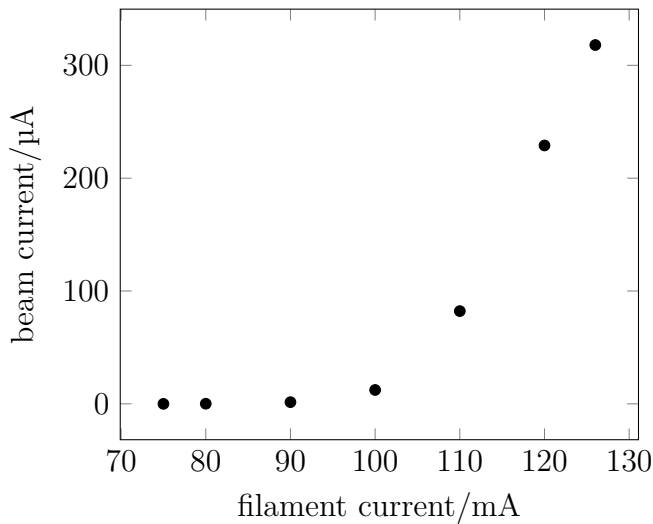


**Figure 8.4:** Beam current dependence on heater current.

### 8.3 Deflection frequency

This section describes a few observations that were made when letting the electron beam interact with a short piece of wire which was mounted to the wobble stick. Originally, we hoped to be able to measure the beam waist, using the knife edge method, i.e. observing the current transported by the beam, while slowly moving a razor blade through the beam path. However the beam is bent, when it passes closely to a conductive part. Whenever, we moved our wire close to the beam, the visible spot on the Phosphorous screen below was distorted. This will probably complicate the measurement of the beam waist in the future. When the wire is connected to an oscilloscope, one can see a sharp increase in voltage, when it is moved into the beam. This can be used to see whether our deflection plates work properly and to test how fast we are able to deflect the beam. If the beam oscillates back and forth on a straight line and crosses the wire on the midway point, we should see a spike in voltage on the wire, which repeats with twice the frequency of the beam. If the wire is not on the midway point, the periods between consecutive spikes should sum up to the period of the beam's oscillation (see fig. 8.5). At low frequencies we have indeed observed

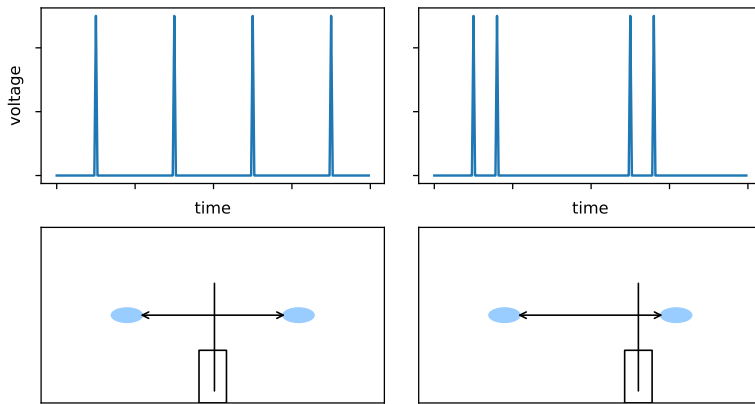


**Figure 8.5:** Observed Voltage-spikes induced by an electron beam that was deflected periodically across a wire. (Arbitrary units)

this behavior. As the frequency is increased, the magnitude of the signal decreases. This is easily explained by the fact that the remain time close to the wire is inversely proportional to the frequency and the amplitude of beams deflection. It was possible to see the spikes up to a frequency of 100 kHz before they were obscured by noise and some other periodical, but so far unexplained artifacts. At high deflection frequencies, the wire may also pick up some signal from the capacitive charging and discharging of the deflection plates and the corresponding oscillating electromagnetic field. In order to be able to see what happens at higher frequencies, a higher beam current and a smaller deflection amplitude would be beneficial. However, the most important factor in order to understand what is happening, is a better focus and a better beam shape.

# 9 Next Steps

To conclude this report, we will point out some of the next steps that need to be taken in order to advance the electron beam setup.

**Beam current stability:** The most important challenge at this moment is the ability to generate a reproducible, stable, and sufficiently strong beam. In order to achieve this, more research on cathodes and their susceptibility to oxygen poisoning needs to be conducted. It may also prove useful to add another high voltage power supply to the setup, in order to tune the filament potential independently from the Wehnelt cylinder.

**Spot size characterisation:** As previously mentioned, our original attempt was, to probe the electron beam's profile using a thin piece of wire on the wobble stick. However, we have observed that the beam got warped, when passing close to conductive materials. Therefore, a different approach is needed.

**Heating mechanism:** As high currents will degrade the filament and cathode, it is desirable to be able to tune the heater current down to 0 mA continuously. Such a power supply needs to support a bias voltage of around  $-2\text{ kV}$ . The current heater (described in section [4.4](#)) has a minimal current of approximately 60 mA. It could be improved by using a potentiometer with a larger resistance range or a variable transformer.

**Lissajous Curves:** Regarding the deflection electronics, the first issue that needs to be addressed, is the fact that it is not possible to produce a clean sine wave, when a bias voltage is applied to the center tapped transformer. Furthermore, it is recommended to implement the over voltage protection described previously with very low capacitance diodes. In the future, the setup should be able to produce Lissajous curves at the  $^{39}\text{K}$  hyperfine transition frequency of 461.7 MHz (or at a frequency of 254 MHz for  $^{41}\text{K}$ ).

# References

- [1] Tobias Tiecke. *Properties of Potassium*. URL: <https://tobiastiecke.nl/archive/PotassiumProperties.pdf> (visited on 05/15/2020).
- [2] Wikipedia Contributors. *Cathode-ray tube - Wikipedia*. Jan. 22, 2021. URL: [https://en.wikipedia.org/wiki/Cathode-ray\\_tube](https://en.wikipedia.org/wiki/Cathode-ray_tube).
- [3] Wolfgang Demtröder. *Experimentalphysik 3*. Springer-Lehrbuch. Berlin, Heidelberg: Springer-Verlag Berlin Heidelberg, 2009. Chap. 2.6.1.
- [4] Frank Philipse. *D14363GY123*. URL: <https://frank.pocnet.net/sheets/186/d/D14363GY123.pdf> (visited on 03/10/2020).
- [5] Jerry C. Whitaker and Fla. [Verlag] CRC Press Boca Raton. *Power vacuum tubes handbook*. Third edition. Electronics handbook series. Boca Raton, FL: CRC Press.
- [6] Chuck deVere. *Cathode-Ray Tubes*. 1969.
- [7] Aviv Keshet and Wolfgang Ketterle. “A Distributed, GUI-based, Computer Control System for Atomic Physics Experiments”. In: *Review of Scientific Instruments* 84.1 (2013), p. 015105.
- [8] Aviv Keshet. *The Cicero Word Generator*. URL: <https://github.com/akeshet/Cicero-Word-Generator> (visited on 02/20/2020).
- [9] Aviv Keshet. *Cicero Word Generator Technical and User Manual*. URL: <http://akeshet.github.io/Cicero-Word-Generator/Cicero%20Technical%20and%20User%20Manual.pdf> (visited on 02/24/2020).
- [10] Microsoft. *Download .NET (Linux, macOS, and Windows)*. URL: <https://dotnet.microsoft.com/download> (visited on 02/24/2020).
- [11] National Instruments. *NI Driver Downloads - National Instruments*. URL: <https://www.ni.com/en-us/support/downloads/drivers.html> (visited on 02/24/2020).
- [12] National Instruments. *NI Software Gives C++ Runtime Error “Terminated in an Unusual Way” - National Instruments*. URL: <https://knowledge.ni.com/KnowledgeArticleDetails?id=kA00Z0000019YOnSAM&l=en-US> (visited on 02/24/2020).
- [13] Rohde & Schwarz. *HM 507*. URL: [https://cdn.rohde-schwarz.com/hameg-archive/HM507\\_english.pdf](https://cdn.rohde-schwarz.com/hameg-archive/HM507_english.pdf) (visited on 03/28/2020).
- [14] FuG Elektronik GmbH. *HVPS Series HCP*. URL: [https://www.fug-elektronik.de/wp-content/uploads/pdf/Datasheets/EN/HCP\\_data\\_sheet.pdf](https://www.fug-elektronik.de/wp-content/uploads/pdf/Datasheets/EN/HCP_data_sheet.pdf) (visited on 03/23/2020).

## References

---

- [15] Myrra SAS. *Data Sheet 44231*. URL: <http://www.farnell.com/datasheets/92205.pdf> (visited on 04/07/2020).
- [16] Murata Power Solutions. *ACA-20PC manual*. URL: <https://www.murata.com/products/productdata/8807023804446/aca20pc.pdf> (visited on 04/07/2020).
- [17] Mini-Circuits. *ZHL-32A Data sheet*. Jan. 22, 2021. URL: <https://www.minicircuits.com/pdfs/ZHL-32A+.pdf>.
- [18] Mini-Circuits. *ZHL-1A Data sheet*. Jan. 22, 2021. URL: <https://www.minicircuits.com/pdfs/ZHL-1A+.pdf>.
- [19] Mini-Circuits. *TC8-1G2+*. URL: <https://www.minicircuits.com/pdfs/TC8-1G2+.pdf> (visited on 05/05/2020).
- [20] Mini-Circuits. *JSPHS-661+ Data Sheet*. URL: <https://www.minicircuits.com/pdfs/JSPHS-661+.pdf> (visited on 05/05/2020).
- [21] Hammond Manufacturing. *1455D601RD*. URL: <https://www.hammfg.com/files/partspdf/1455D801RD.pdf> (visited on 05/05/2020).